

Cell-perceived substrate curvature dynamically coordinates the direction, speed, and persistence of stromal cell migration

Citation for published version (APA):

Werner, M., Petersen, A., Kurniawan, N., & Bouten, C. (2019). Cell-perceived substrate curvature dynamically coordinates the direction, speed, and persistence of stromal cell migration. *Advanced Biosystems*, 3(10), Article 1900080. <https://doi.org/10.1002/adbi.201900080>

DOI:

[10.1002/adbi.201900080](https://doi.org/10.1002/adbi.201900080)

Document status and date:

Published: 01/10/2019

Document Version:

Publisher's PDF, also known as Version of Record (includes final page, issue and volume numbers)

Please check the document version of this publication:

- A submitted manuscript is the version of the article upon submission and before peer-review. There can be important differences between the submitted version and the official published version of record. People interested in the research are advised to contact the author for the final version of the publication, or visit the DOI to the publisher's website.
- The final author version and the galley proof are versions of the publication after peer review.
- The final published version features the final layout of the paper including the volume, issue and page numbers.

[Link to publication](#)

General rights

Copyright and moral rights for the publications made accessible in the public portal are retained by the authors and/or other copyright owners and it is a condition of accessing publications that users recognise and abide by the legal requirements associated with these rights.

- Users may download and print one copy of any publication from the public portal for the purpose of private study or research.
- You may not further distribute the material or use it for any profit-making activity or commercial gain
- You may freely distribute the URL identifying the publication in the public portal.

If the publication is distributed under the terms of Article 25fa of the Dutch Copyright Act, indicated by the "Taverne" license above, please follow below link for the End User Agreement:

www.tue.nl/taverne

Take down policy

If you believe that this document breaches copyright please contact us at:

openaccess@tue.nl

providing details and we will investigate your claim.

Cell-Perceived Substrate Curvature Dynamically Coordinates the Direction, Speed, and Persistence of Stromal Cell Migration

Maïke Werner, Ansgar Petersen, Nicholas A. Kurniawan,* and Carlijn V. C. Bouten

Adherent cells residing within tissues or biomaterials are presented with 3D geometrical cues from their environment, often in the form of local surface curvatures. While there is growing evidence that cellular decision-making is influenced by substrate curvature, the effect of physiologically relevant, cell-scale anisotropic curvatures remains poorly understood. This study systematically explores the migration behavior of human bone marrow stromal cells (hBMSCs) on a library of anisotropic curved structures. Analysis of cell trajectories reveals that, on convex cylindrical structures, hBMSC migration speed and persistence are strongly governed by the cellular orientation on the curved structure, while migration on concave cylindrical structures is characterized by fast but non-aligned and non-persistent migration. Concurrent presentation of concave and convex substrates on toroidal structures induces migration in the direction where hBMSCs can most effectively avoid cell bending. These distinct migration behaviors are found to be universally explained by the cell-perceived substrate curvature, which on anisotropic curved structures is dependent on both the temporally varying cell orientation and the 3D cellular morphology. This work demonstrates that cell migration is dynamically guided by the perceived curvature of the underlying substrate, providing an important biomaterial design parameter for instructing cell migration in tissue engineering and regenerative medicine.

1. Introduction

In the body, cells migrate through the extracellular matrix, whose microstructure defines physical boundary conditions for various vital cell activities, including cell migration. It is well established that cell migration is influenced by topographical cues from the environment.^[1–4] In vitro experiments using protein tracks and micro-/nano-fabricated grooves and ridges have convincingly demonstrated that the migration of adherent cells is guided by anisotropic topographical features (i.e., structures with different geometric properties in different directions) of the substrate—a phenomenon termed “contact guidance.”^[5–11] Such studies have yielded important insights into the fundamental mechanisms underlying cell migration, which contribute toward our understanding of morphogenesis and disease development, such as in cancer metastasis.^[12,13] However, in many cases, pre-existing structures in tissues and organs present an architecture that is not

captured by the abovementioned two-dimensional approaches, for example, in the form of collagen fiber bundles, blood vessel walls, and cavities.^[14–16] These structures are typically characterized by mesoscale (i.e., $\approx 100\ \mu\text{m}$ to mm) surface curvatures. Such curved surfaces are also often encountered by cells in implanted biomaterials and scaffolds for tissue engineering, whereby cell migration and infiltration into the constructs is a crucial step for the success of the intervention.^[17]


The profound effect of surface curvatures on cell behavior has only started to be appreciated. Park et al. observed that, on polydimethylsiloxane (PDMS) membranes with concave or convex spherical structures, cells actively migrate out of concave pits but attach and proliferate on convex structures.^[18] In a previous study, we demonstrated that cells exhibit different attachment morphologies on convex and concave spherical substrates.^[19] Convex spherical substrates force the cells to adopt a bent shape, inducing a compressive pressure by the actin cytoskeleton on the nucleus. On the other hand, cells on concave spherical surfaces lift their bodies upward, minimizing the contact area with the substrate and nucleus compression. Furthermore, cell migration speed was found to be significantly higher on concave spherical

M. Werner, Dr. N. A. Kurniawan, Prof. C. V. C. Bouten
Department of Biomedical Engineering
Eindhoven University of Technology
5612 AJ Eindhoven, The Netherlands
E-mail: N.A.Kurniawan@tue.nl

M. Werner, Dr. N. A. Kurniawan, Prof. C. V. C. Bouten
Institute for Complex Molecular Systems
Eindhoven University of Technology
5600 MB, Eindhoven, The Netherlands

Dr. A. Petersen
Julius Wolff Institute
Charité—Universitätsmedizin Berlin
Augustenburger Platz 1, D-13353 Berlin, Germany

Dr. A. Petersen
Berlin-Brandenburg Center for Regenerative Therapies
Charité—Universitätsmedizin Berlin
Augustenburger Platz 1, D-13353 Berlin, Germany

 The ORCID identification number(s) for the author(s) of this article can be found under <https://doi.org/10.1002/adbi.201900080>.

© 2019 The Authors. Published by WILEY-VCH Verlag GmbH & Co. KGaA, Weinheim. This is an open access article under the terms of the Creative Commons Attribution License, which permits use, distribution and reproduction in any medium, provided the original work is properly cited.

DOI: 10.1002/adbi.201900080

surfaces than on convex spherical surfaces.^[19] On sphere-with-skirt surfaces (i.e., a convex spherical cap, surrounded by a concave draping skirt), mouse embryonic fibroblasts were shown to primarily remain in the concave area of the substrate and migrate around the geometrical structure in the azimuthal direction.^[20] Recently, these findings were further corroborated by Pieuchot et al. by plating cells on a substrate of a continuous landscape of spherical convex and concave topographies, demonstrating that the interplay between cell contractility and nuclear mechanics is responsible for active cell migration toward the concave valleys.^[21]

Physiologically relevant structures typically contain anisotropic (i.e., direction-dependent) surface curvatures, both convex (e.g., matrix and scaffold fibers/studs) and concave (e.g., channel-like pores). Anisotropic structures generally have unequal curvatures in different directions. This is particularly relevant in complex scaffold designs for tissue engineering, which can be produced with high accuracy and control using additive manufacturing techniques. In a mathematically designed approach, scaffolds can be designed with predefined Gaussian curvature distributions. However, to effectively employ specific scaffold architectures for guiding cell migration and orientation, prior knowledge on how cells respond to basic geometries is necessary. In the case of convex cylindrical structures, fibroblasts and smooth muscle cells have been shown to orient toward the longitudinal axis of the cylinders, that is, the direction of minimal curvature.^[10,22] Our recent work demonstrated that this guidance effect by convex mesoscale cylindrical structures can even overrule co-existing nanoscale contact guidance cues.^[23] While these early findings start to uncover the importance of considering anisotropic substrate curvatures, how they translate to cell migration behavior on concave anisotropic structures or even more complex geometries encountered in tissues and biomaterial scaffolds remains unknown.

In this work, we address this outstanding gap by investigating the migration dynamics of human bone marrow stromal cells (hBMSCs), a cell type that plays an important role in the regeneration of many tissues,^[24] on a library of anisotropic concave and convex structures with systematically varying dimensions. Cell migration trajectories reveal distinct migration modes that are universally determined by the sign and magnitude of the “cell-perceived” substrate curvature. Moreover, the cells dynamically adjust their migration mode to avoid cell bending due to substrate curvature but apply different strategies to do so on concave and convex surfaces. The findings are relevant for understanding cell organization in complex geometric environments and can inspire new strategies for the geometrical design of scaffolds for tissue engineering, especially for guiding directed cell migration.

2. Results and Discussion

2.1. hBMSC Migration Direction, Persistence, and Speed on Anisotropic Curved Structures are Affected by the Sign and Magnitude of Surface Curvature

To systematically study the effect of anisotropic substrate curvature on cell migration, we microfabricated a PDMS chip containing arrays of convex and concave cylindrical structures with diameters (d) ranging from 250 to 1000 μm , corresponding

to principal curvatures κ of $\pm 1/125$ to $\pm 1/500 \mu\text{m}^{-1}$ (negative sign for concave; positive for convex). hBMSCs were seeded on these chips for 3 h and their 3D migration on the structures was followed using time-lapse confocal microscopy for 48 h. A remarkable difference in the migration behavior of the cells was observed on convex and concave cylindrical surfaces (Movies 1 and 2, Supporting Information). The movies and migration tracks showed that, on concave cylindrical surfaces, the cells frequently changed migration direction and the overall migration pattern showed no angular preference (Figure 1a). In contrast, cell migration on convex cylindrical surfaces was persistently directed along the longitudinal axis of the cylinder (Figure 1b). To quantify this anisotropic migration, we calculated an anisotropy index dx/dy : the ratio of migration distance in the longitudinal (x) and circumferential (y) directions of the cylinders.^[23] Consistent with our qualitative observations, on convex surfaces dx/dy exceeds 1 on all cylinder sizes, indicating an anisotropic migration towards the longitudinal cylinder axis. In contrast, dx/dy on concave structures and flat surfaces is close to 1, indicating isotropic migration (Figure 1c). Importantly, dx/dy depended not only on the sign of curvature (convex vs concave) but also on the magnitude of the principal curvature κ on convex surfaces. No significant difference in migration directionality was found on concave cylindrical surfaces compared to on flat surfaces, irrespective of the cylinder size.

The second characteristic difference between cell migration on concave and convex cylindrical surfaces that we observed is that hBMSCs migrate more persistently on convex surfaces (Movies 1 and 2, Supporting Information). To quantify the migration persistence, we calculated the persistence time t_p , that is, the duration a cell continues to migrate in a certain direction (see Section 4). Indeed, t_p was significantly higher in cells migrating on convex cylindrical surfaces compared to those on concave cylindrical surfaces (at $\kappa < 1/500 \mu\text{m}^{-1}$) (Figure 1d). Compared to the situation on flat surfaces ($\kappa = 0$), cells changed migration direction significantly more frequently on highly curved concave cylinders ($\kappa = -1/125$ and $-1/175 \mu\text{m}^{-1}$).

Migration persistence has been shown to universally correlate with cell migration speed v for various cell types in 2D and 3D in vitro as well as in vivo situations.^[25] This correlation was argued to arise from the advection of polarity cues and actin flows that mediate cell polarization and migration. In contrast to this expected correlation, in our experiments we found that v was consistently higher on concave cylindrical surfaces (i.e., where t_p is low) than on convex cylindrical surfaces and on flat surfaces (i.e., where migration is more persistent) (Figure 1e). In addition, on convex surfaces, v was constant regardless of κ , while t_p increased with increasing κ . These findings suggest that anisotropic curved substrates provoke the cells to adopt fundamentally different migration modes, resulting in an apparent violation of the previously reported persistence–speed correlation.

2.2. Direction-Dependent Perceived Curvature Affects Cell Migration Orientation on Convex, but not Concave Cylindrical Substrates

On cylindrical structures, the curvature that the cell perceives, k , is dependent on the cellular orientation on the cylinder, θ

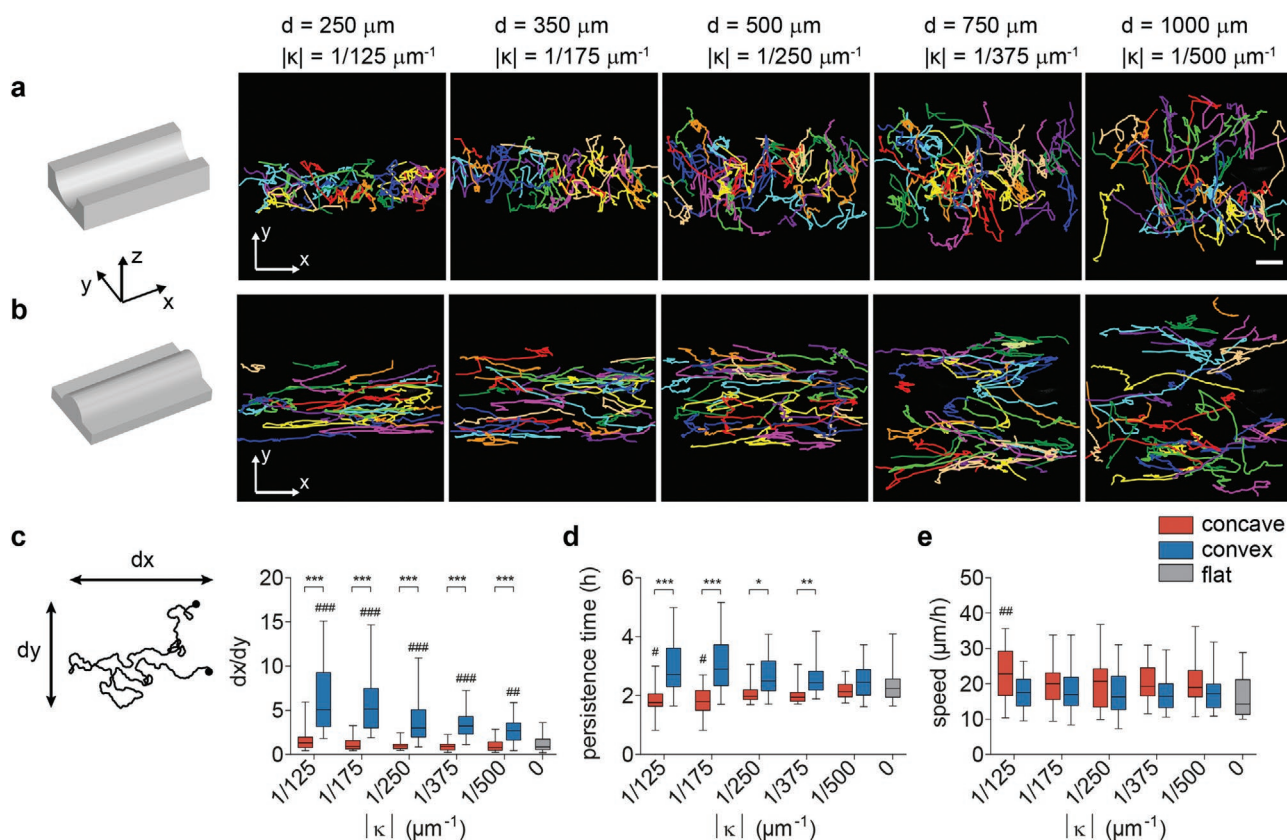


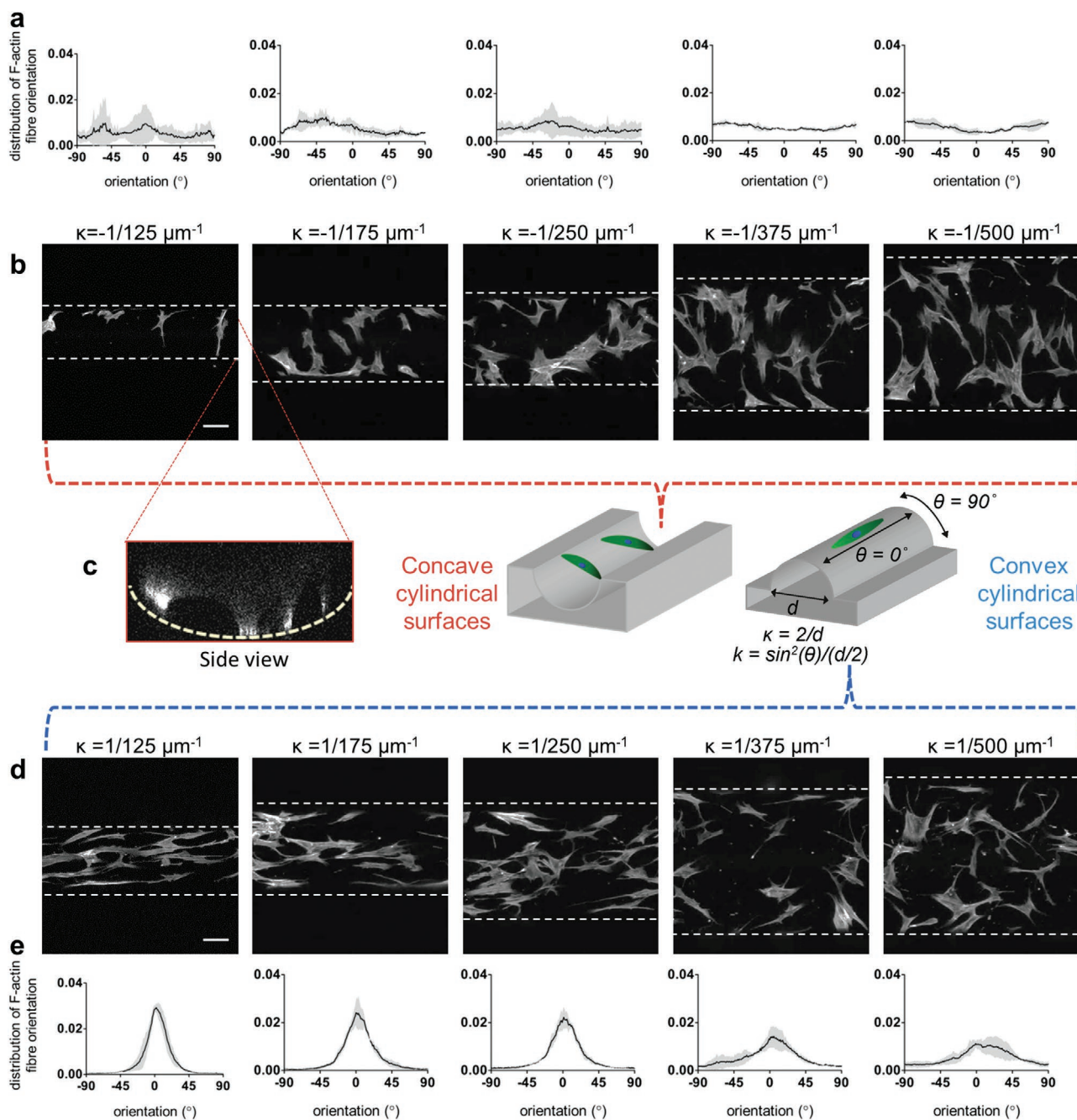
Figure 1. hBMSCs migration on cylindrical surfaces. Migration tracks of hBMSC migration on a) concave and b) convex cylindrical structures with diameters d of 250–1000 μm (corresponding to $|\kappa| = 1/125\text{--}1/500 \mu\text{m}^{-1}$), as seen from the top (in the x - y plane). Tracks of different cells ($n \geq 26$ per experimental group) are depicted by different colors. Scale bar = 100 μm . Migration tracks of hBMSC migration on a flat surface can be found in Figure S1, Supporting Information. c) Anisotropy index dx/dy , as calculated from the ratio of cell migration along the longitudinal (dx) and circumferential directions (dy) on convex and concave cylindrical surfaces as well as on control flat surfaces. d) The duration a cell persistently migrates in the same direction, and e) the migration speed, as analyzed from the migration tracks. Data are shown as box and whisker plots. Whiskers represent the 5 and 95 percentiles ($n \geq 26$ per experimental group), where *, **, and *** indicate a significant difference between values on convex and concave cylinders of the same diameter and #, ##, and ### indicate a significant difference in comparison to flat surfaces ($p < 0.05$, $p < 0.01$, and $p < 0.001$, respectively).

(see schematic illustration in **Figure 2**). For cylindrical structures, $k(d, \theta)$ is given by $k = \sin^2(\theta)/(d/2)$. This direction-dependent perceived curvature k is zero along the longitudinal axis of the cylinder ($\theta = 0^\circ$) for both concave and convex structures. However, when the cell is oriented perpendicular to the longitudinal axis (i.e., in the circumferential direction of the cylinder), the perceived curvature of the cell equals the principal curvature of the cylinder (i.e., as $|\theta| \rightarrow 90^\circ$, $k \rightarrow \kappa$). To better understand the cells' adhesion strategy when presented with such direction-dependent substrate curvature, we examined their orientation with respect to the cylinder orientation and F-actin organization.

Cells on convex surfaces elongated and aligned along the longitudinal axis of the cylinder (Figure 2d,e). This effect becomes increasingly pronounced with decreasing cylinder sizes (or increasing κ). This positive-curvature-mediated cell alignment can be explained by the cells' aversion to bending.^[23] It was proposed before in a mechanical model that cells with mature stress fibers orient themselves in a direction of least curvature to avoid bending of stress fibers.^[26,27] On convex cylindrical surfaces, cells try to minimize cell bending by aligning (and migrating) in the $\theta = 0^\circ$ direction, where $k = 0$. This curvature-

avoidance behavior is therefore expected to be dependent on $|\kappa|$, as cells would increasingly try to remain aligned in the $k = 0$ direction with increasing κ . Indeed, the highest directionality (dx/dy) and persistence (t_p) were seen on the smallest cylinders (Figure 1c,d). Time-lapse movies demonstrated that the cells showed the typical extension and contraction dynamics, characteristic of lamellipodia-mediated mesenchymal migration on 2D surfaces,^[28] in a persistent manner along the longitudinal cylinder axis (Movie 3, Supporting Information). In this situation, the cells can be expected to follow the previously reported correlation between migration speed and persistence.^[25]

On concave cylindrical surfaces, in theory cells have two options for avoiding bending: they can either align in the longitudinal direction ($\theta = 0$), similar to what they do on convex surfaces, or they can make use of the unconstrained open space in the third dimension (z) by lifting their bodies off of the substrate and stretching upward, like what they do on concave spherical pits.^[19] As shown in Figure 2c, hBMSCs preferred the latter strategy; they arched off the concave surfaces, with limited contact area with the substrate. Similar detachment and upward stretching on concave surfaces have been shown for single smooth muscle cells (SMC) and for SMC sheets.^[29,30] In



Curvature guidance

Figure 2. hBMSCs orientation and morphology on concave and convex cylindrical surfaces. Distributions of F-actin fiber orientation, where 0° indicates the longitudinal direction of the cylinders and representative immunofluorescence images of cells showing F-actin staining on a,b) concave and d,e) convex cylindrical substrates of varying principal curvatures κ . Scale bar = $100 \mu\text{m}$. Dashed lines indicate the contour of the cylindrical surfaces. Data are shown as mean \pm standard deviation ($n = 3$ images per experimental group, $n > 38$ cells per experimental group). c) An example side-view image of a cell on a concave cylinder of diameter $250 \mu\text{m}$.

mouse embryonic fibroblasts (MEFs) it was shown that apical stress fibers avoid bending by lifting away from the surface and bridge over a concave area of a curved surface.^[20] This implies that the curvature that cells perceive is additionally influenced by the attachment morphology on concave substrates.

Moreover, the upward lifting of the cell body did not happen in a preferred direction, thus leading to a random orientation (Figure 2a,b) and an isotropic migration trajectory (Figure 1c). Indeed, we observed that the cells stretched with long, thin cell-extensions in various directions that resulted in non-persistent,

undirected cell migration behavior (Movie 4, Supporting Information). Another important consequence is that the cell-substrate contact area is reduced to distinct adhesion points at the periphery of the cell, similar to the adhesion morphology previously reported in spherical pits.^[19] This could promote faster remodeling of the cytoskeleton and focal adhesions,^[31] and thus faster migration.^[19] This unique coping mechanism may therefore explain the significantly lower t_p on concave cylindrical surfaces compared to on convex surfaces (Figure 1d), despite the higher migration speed (Figure 1e).

2.3. hBMSCs Adjust Their Migration Speed in Direct Response to the Temporally Varying Cell-Perceived Substrate Curvature

Since the perceived substrate curvature k is likely to continuously vary along the migration trajectories of the cells, it becomes necessary to analyze each cell track in greater detail. The migration tracks were analyzed from time-lapse movies where the centroids of cells were detected at every timeframe and tracked. By analyzing the change in position coordinates between the frames, we extracted the instantaneous migration speed $v(t)$, direction $\theta(t)$, and turn angle of every migra-

tion track segment of all cell tracks (see Section 4). On flat surfaces, the ensemble distribution of migration direction θ was constant, indicating that cells do not show a preferred orientation. The ensemble distribution of migration speed v was similarly unaffected by θ (Figure 3a), as expected for completely isotropic behavior. On convex cylinders, v was strongly affected by θ ; speed was significantly reduced when the migration was directed away from the longitudinal axis of the cylinder (Figure 3c and Figure S2, Supporting Information). Moreover, cell migration was predominantly oriented along the cylinder axis ($\theta = 0^\circ$) (Figure 2d,e). On concave cylinders, cells did not show a dominant migration direction like on flat surfaces, but v seemed to be slightly higher at directions around $|\theta| = 90^\circ$ (Figure 3b and Figure S2, Supporting Information).

To parameterize this direction-dependence, we classified the track segments to be “aligned” when θ lies within 30° from 0° (i.e., in the direction where $k \approx 0$) and “non-aligned” otherwise. This classification revealed diametrically opposite migration behaviors on convex ($\kappa > 0$) and concave ($\kappa < 0$) surfaces; on convex cylinders, the ensemble-averaged speed \bar{v} was significantly higher when the migration was aligned than when non-aligned, whereas on concave cylinders, \bar{v} was significantly higher when non-aligned instead (Figure 3d). Three important

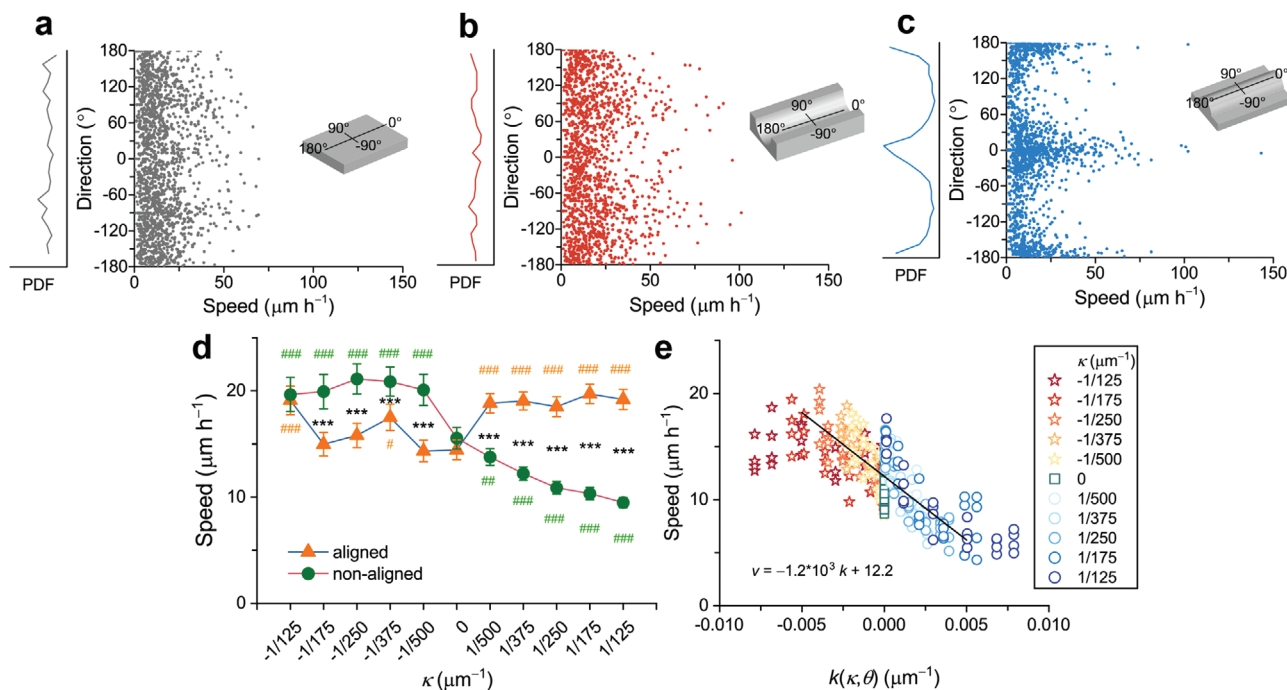


Figure 3. Direction-dependent hBMSCs migration speed on cylindrical surfaces. The migration speed of every track segment is plotted against the respective migration direction on a) flat surfaces, b) concave cylindrical structures with $d = 500 \mu\text{m}$ (corresponding to $\kappa = -1/250 \mu\text{m}^{-1}$), and c) convex cylindrical structures with $d = 500 \mu\text{m}$ (corresponding to $\kappa = 1/250 \mu\text{m}^{-1}$). Migration track segments of 30 cells per experimental group were analyzed. The left panels show the ensemble probability distribution functions (PDF) of the migration direction, with 0° and $\pm 180^\circ$ indicating the longitudinal direction of the cylinders and $\pm 90^\circ$ indicating the circumferential direction of the cylinders. See Figure S2, Supporting Information, for the complete analysis for all cylinder diameters ($d = 250\text{--}1000 \mu\text{m}$). d) Average migration speeds when the cells are aligned (yellow triangles) and when non-aligned (green circles) for varying cylinder principal curvatures κ ($\kappa < 0$: concave; $\kappa > 0$: convex). A track segment is classified as “aligned” when the instantaneous migration direction θ lies within 30° from 0° or from $\pm 180^\circ$ and “non-aligned” otherwise. Data are shown as mean \pm 95% confidence interval, where *** indicates a significant difference between \bar{v}_{aligned} and $\bar{v}_{\text{non-aligned}}$ ($p < 0.001$) and #, ##, and ### indicate a significant difference in comparison to flat surfaces ($p < 0.05$, $p < 0.01$, and $p < 0.001$, respectively). e) Mean speed as a function of the perceived curvature k . The cell migration speeds of the track segments on concave cylinders, convex cylinders, and flat surfaces (each condition indicated by different colors) follow a master relation, showing a negative correlation with the perceived curvature k , as shown by the black trend line and the associated equation.

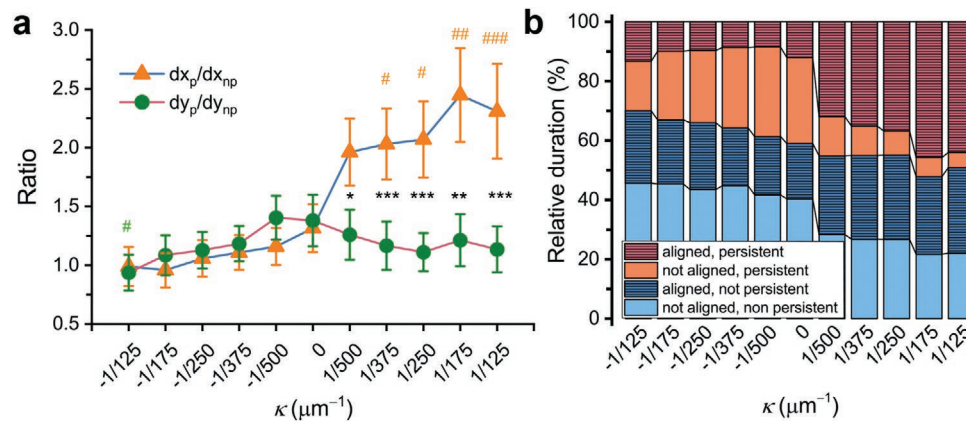


Figure 4. Migration persistence of hBMSCs on cylindrical surfaces depends on cell orientation. a) The ratio between migration distance in x - and y -directions (dx and dy , respectively) during the persistent (p) and non-persistent (np) phases of the migration trajectories, on cylindrical substrates of varying principal curvatures κ . Data are shown as mean \pm 95% confidence interval, where *, **, and *** indicate a significant difference between dx_p/dx_{np} and dy_p/dy_{np} and #, ##, and ### indicate a significant difference in comparison to flat surfaces ($p < 0.05$, $p < 0.01$, and $p < 0.001$, respectively). b) The relative durations of the various phases of migration phenotypes. Migration tracks of ≥ 26 cells per experimental group were analyzed. Every individual migration track consists of a multitude of track segments (see Section 4).

observations are particularly illuminating. First, on convex surfaces, \bar{v}_{aligned} (i.e., in the direction where $k \approx 0$) was relatively constant regardless of κ , but $\bar{v}_{\text{non-aligned}}$ decreased with increasing κ (and therefore k). This is a clear indication that cells sense and respond to the perceived direction-dependent substrate curvature on convex cylindrical surfaces. Second, $\bar{v}_{\text{non-aligned}}$ on concave surfaces was constant regardless of κ , but was significantly higher than $\bar{v}_{\text{non-aligned}}$ on convex surfaces of the same $|k|$ (Figure 3d, green circles). Third, \bar{v}_{aligned} on convex surfaces was higher compared to both, \bar{v} on flat and \bar{v}_{aligned} on concave surfaces. The former comparison (\bar{v}_{aligned} on convex vs \bar{v} on flat) is consistent with the idea that v is correlated with migration persistence,^[25] as the cells migrate more persistently on convex than on flat surfaces (Figure 1d), but the latter comparison (\bar{v}_{aligned} on convex vs \bar{v}_{aligned} on concave) again corroborates distinct migration modes on convex and concave surfaces.

To conclusively test whether cell migration speed depends on the perceived curvature k , we binned the cell track segments according to θ and plotted the mean speed per bin as a function of the direction-dependent perceived curvature k in Figure 3c. Strikingly, the ensemble data for all concave and convex cylinders as well as flat surfaces coincided into a master relation, characterized by a negative linear dependency between migration speed and the perceived substrate curvature k in the range of $-0.005 < k < 0.005 \mu\text{m}^{-1}$. This remarkable universality demonstrates that the various migration modes of cells on curved surfaces are driven by the perceived substrate curvature k .

Since on cylindrical surfaces, k varies with migration direction, we then asked whether this implies that cells continually probe the substrate curvature and “update” their migration mode accordingly. To test this hypothesis, we constructed heat maps of the migration speed versus direction and checked whether individual cell trajectories explore the whole accessible phase space or stay within a narrow window. We indeed found that cells sampled a wide range of the speed versus direction phase space (a representative sampling from one randomly picked cell is shown in Figure S3, Supporting Informa-

tion), indicating that cells dynamically adjust their migration behavior depending on k .

2.4. Migration Persistence Depends on Cell Migration Direction on Convex Cylindrical Substrates

Having established that the instantaneous migration speed is dependent on the direction-dependent perceived curvature, we next investigated whether migration persistence is similarly dependent on the migration direction. To separate these two parameters, we examined the migration distance during the persistent (p) and non-persistent (np) phases along the longitudinal (dx) and circumferential directions (dy) (see also the schematic illustration in Figure 1c). If migration persistence is independent of direction, then the ratio dx_p/dx_{np} should be close or identical to dy_p/dy_{np} , as is the case for flat surfaces ($\kappa = 0$ in Figure 4a). Interestingly, we found that on convex cylinders ($\kappa > 0$), the directionality of the migration during the persistent phases was enhanced with respect to the non-persistent phases, but only in the longitudinal direction (dx_p/dx_{np}) and not in the circumferential direction (dy_p/dy_{np}) (Figure 4a). This indicates that migration persistence is promoted on convex cylindrical surfaces along the cylinder axis. In contrast, on concave cylinders ($\kappa < 0$), there was a slight, statistically insignificant increase in the y -direction (i.e., non-aligned direction) during the persistent phases (dy_p/dy_{np}). To further define the link between migration direction and persistence, we quantified the relative durations that the cells spend in persistent versus non-persistent and aligned versus non-aligned phases and their residence times in these phases. As shown in Figure 4b and Figure S4, Supporting Information, large positive κ increases the likelihood that a cell migrates in a persistent and aligned manner. On the other hand, large negative κ is associated with dominantly non-persistent migration and non-aligned migration during the rare persistent phases. These results indicate that the principal curvature of the cylindrical substrates affects both migration persistence and alignment.

Together, these findings suggest that the likelihood to change the direction of migration on convex cylindrical surfaces might in fact be dependent on the perceived curvature k by the cell.

To test this hypothesis, we performed a probabilistic analysis of the turn angles as a function of migration direction (Figure S5, Supporting Information). The result confirms that when cells migrate along the longitudinal axis of the convex cylinders, there is a higher likelihood that the cells continue to migrate in that direction (i.e., low turn angle), leading to a higher migration persistence than when the cells migrate along other directions. This direction-dependent migration mode is not observed on concave cylinders and on flat substrates. To check how this propensity of turning affects migration persistence over time, we constructed probabilistic kymographs from the ensemble trajectories given specified starting conditions (see Section 4). The analysis shows that on concave cylindrical structures, the migration persistence is constant across all migration directions (Figure S6a,d, Supporting Information), likely because the cells lift upward and adopt a morphology with limited adhesion to the curved substrates. In contrast, on convex cylinders, the duration over which migration direction is maintained is direction-dependent; persistence time is higher when cells are aligned than when cells are non-aligned (Figure S6c,f, Supporting Information). These findings demonstrate that migration persistence is affected by the perceived substrate curvature k .

Our results show that the distinct attachment morphologies on concave and convex cylindrical substrates have a substantial and non-trivial effect on the migration direction, persistence, and speed of cells on these substrates. It is worth noting that our experimental results are in direct contrast to the findings of a recently proposed computational model, which predicted more persistent migration on concave cylinders compared to on convex cylinders,^[32] likely because these distinct attachment strategies were not accounted for. In the model, concave surfaces provide a constrained geometry that facilitates cell protrusion forces along the longitudinal axis and therefore a more persistent migration on concave surfaces. However, the model assumes that the cell body remains attached to the curved surface and therefore does not take into account the upward stretching of the cells, which we show here to play a crucial role in hBMSC adhesion and migration on concave structures.

It is tempting to speculate that other cell types with mesenchymal phenotypes comparable to hBMSCs, such as fibroblasts,^[33] may behave similarly. Vascular smooth muscle cells were for instance shown to lift their cell body upward on concave structures in a single cell (in micro-wells and microgrooves, radii = 50–125 μm)^[29] as well as in multi-cell sheet configuration (in micro-channels, radii = 150–500 μm).^[30] It is important to note, however, that other cell types might behave differently. For example, there is evidence that endothelial cells, which naturally line the lumen of cavities and vessels in the body with a cortical cytoskeleton and thin stress fibers, remain fully adhered to concave micro-wells and microgrooves (radii = 50–125 μm).^[29] Interestingly, endothelial cells have also been shown to circumferentially wrap around convex fibers with diameters ranging from 2 to 20 μm ,^[34,35] rather than aligning in the longitudinal direction. T-lymphocytes,

which exhibit amoeboid migration mode,^[36] also do not lift upward on concave surfaces and have been shown to preferentially migrate in concave areas on a sinusoidal wave substrate (wavelength sinusoid 20–160 μm , amplitude 10 μm).^[37] Xi et al. demonstrated that epithelial Madin–Darby canine kidney cells (MDCK) can collectively migrate into concave microtubes ($d = 25\text{--}250 \mu\text{m}$) and form tubular epithelial cell sheets inside the tubes.^[38] Maechler et al. recently cultured other epithelial cell lines, MDCK and J3B1A, in concave tubes ($d = 269 \pm 13 \mu\text{m}$ or $428 \pm 24 \mu\text{m}$). They showed that the monolayers of both cell lines detached from the tube; however, the J3B1A monolayer detached at a slower rate than the MDCK monolayer. This detachment was driven by cellular contractile stresses.^[39] The studies discussed above highlight that the cellular response toward substrate curvatures is highly dependent on both the characteristics of the cell (such as size and contractility) and the characteristics of the structure (size and geometry). As such, caution should be taken when translating the results of the present study, solely focusing on the single-cell migration of hBMSCs, to other cell types. The experimental platform presented here, however, provides an ideal platform to systematically study the response of many different cell types as well as different cell densities toward a wide variety of substrate curvatures in the future. It remains to be investigated whether the insights obtained from our results can be used to explain the directed cell migration along curved structures in vivo, for example, in the context of endothelialization, wound healing, and cancer cell invasion. Our study reveals the importance of considering feature sizes in understanding cell adhesion and migration responses. It was shown before that hBMSCs align along microgrooves smaller than their size,^[40–42] whereas here we demonstrate that hBMSCs exhibit undirected cell orientation and migration on concave cylindrical surfaces larger than their size. It is plausible that when the microgrooves are smaller than the cell size, cells align due to contact-guidance response, but when the concave substrate exceeds a certain diameter, they can lift upward and migrate with no preferential direction.

2.5. hBMSCs Dynamically Adjust Their Migration Direction in Response to Anisotropic Substrate Curvature

While we have so far focused on fiber- or tube-like cylindrical structures, where $k \geq 0$ (convex) or $k \leq 0$ (concave), more complex geometries in biomaterials and scaffolds can concurrently present both positive and negative curvatures to the cells.^[43–45] Thus, we next studied structures that contain both convex and concave surfaces in different directions. We seeded hBMSCs on the saddle point of a torus ring with a diameter of 750 μm . In this structure, $k = -\kappa$ (concave) when $\theta = 0^\circ$, and $k = +\kappa$ (convex) when $\theta = \pm 90^\circ$ (Figure 5a). Here, cells have the option to migrate over the hill in the convex direction ($k > 0$), move diagonally over the structure, span upward in the concave direction ($k < 0$) or any other state in between. We observed that both the cell's orientation (Figure 5b) and migration (Figure 5c) were primarily directed over the concave gap of the torus. Comparison between the migration data on the torus with that on concave and convex cylinders of the same

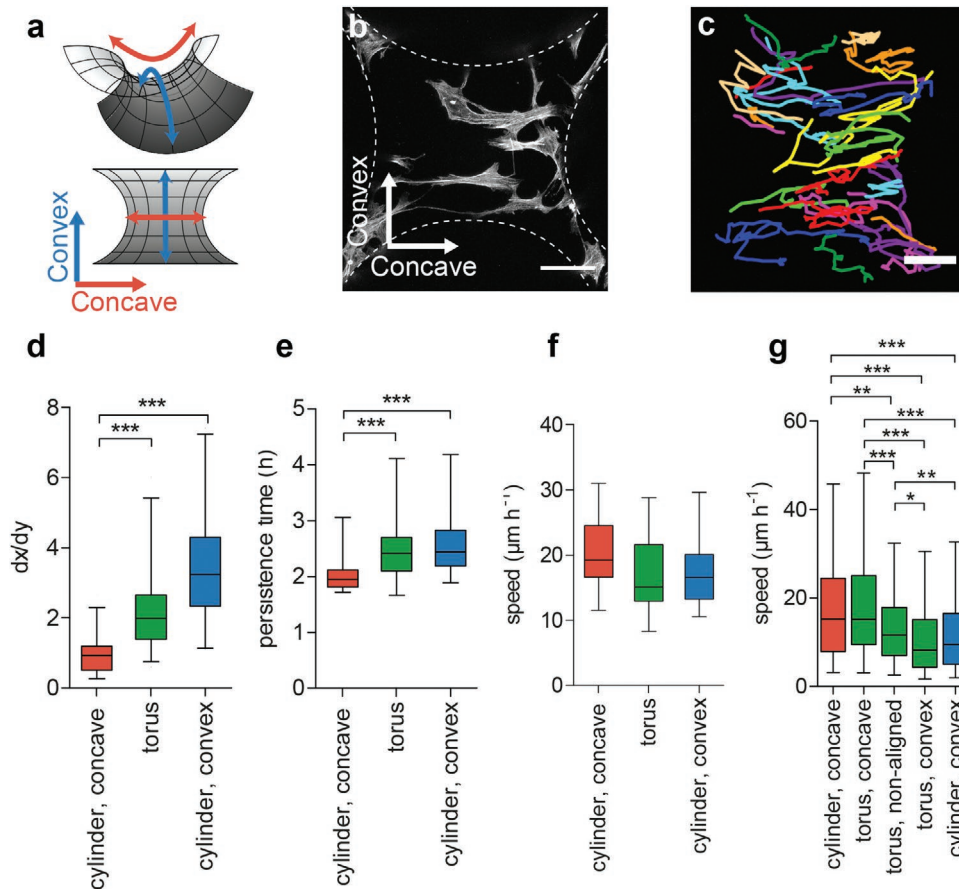


Figure 5. hBMSO organization and migration on a torus. a) The inside of a torus is convex in one direction (here in the vertical direction) and concave in the perpendicular direction (horizontal direction), while the magnitude of the principal curvatures is equal. b) hBMSOs stretch over the concave well of the torus (d torus ring = $750 \mu\text{m}$, corresponding to $|k| = 1/375 \mu\text{m}^{-1}$); F-actin in grey. Scale bar = $100 \mu\text{m}$. Dashed lines indicate the contour of the imaged toroidal surface. Note that only the center area around the central saddle point is displayed here. c) Migration tracks of hBMSO migration on a torus structure ($d = 750$), as seen from the top (in the x - y plane). Tracks of different cells ($n = 27$) are depicted by different colors. Scale bar = $100 \mu\text{m}$. d) Migration directionality, e) persistence, and f) speed analyzed from the complete migration tracks on convex cylinders, concave cylinders, and torus ($d = 750 \mu\text{m}$, $n > 27$ cells, on all geometries). Data are shown as box and whisker plots. Whiskers represent the 5 and 95 percentiles. g) Direction-dependent migration speed on torus and cylindrical structures ($d = 750 \mu\text{m}$). All migration track segments on the torus structures were categorized and classified as “concave” (θ lies within 30° from 0° or from $\pm 180^\circ$), “convex” (θ lies within 30° from $\pm 90^\circ$), and “non-aligned” otherwise. The average speed of the categorized track segments on the torus structures is shown in green and compared to the average migration speed of track segments directed in the $\theta = \pm 90^\circ$ direction on concave (in red) and convex (in blue) cylindrical structures. Error bars = 95% confidence interval.

diameter ($d = 750 \mu\text{m}$) showed that the migration anisotropy index dx/dy on the torus is in between the indexes on concave and convex cylinders. On torus structures, the anisotropy index is significantly higher than that on concave cylinders (Figure 5d). The migration persistence t_p on the torus resembled that on convex cylinders and is significantly higher than that on concave cylinders (Figure 5e). This suggests that cells turn away from the convex direction and orient and migrate in the concave direction of the saddle point.

We note that the average migration speed of the complete cell tracks is not significantly different on torus structures as compared to concave and convex cylindrical structures (Figure 5f). Since the curvature that the cell perceives on the torus-saddle structure can change from concave to convex depending on the cellular orientation, we questioned whether the migration speed is also direction-dependent on torus structures. To test this, we classified the track segments as “concave” when θ

lies within 30° from 0° , “convex” when θ lies within 30° from $\pm 90^\circ$, and “non-aligned” otherwise. We found that the speed \bar{v}_{concave} is larger than $\bar{v}_{\text{non-aligned}}$, which is larger than \bar{v}_{convex} on torus structures (Figure 5f, in green). Furthermore, \bar{v}_{concave} on torus is comparable to \bar{v}_{concave} on concave cylinders of the same κ ($k = -1/375 \mu\text{m}^{-1}$, i.e., speed of the track segments directed in the concave direction [$\theta = \pm 90^\circ$]), and \bar{v}_{convex} on torus is comparable to \bar{v}_{convex} on cylinders of the same κ ($k = 1/375 \mu\text{m}^{-1}$, i.e., speed of the track segments directed in the convex direction [$\theta = \pm 90^\circ$]). These are in agreement with the k -dependence we observed on cylindrical surfaces (Figure 3e) and therefore corroborate the generality of the distinct migration modes on curved substrates. We also found that each cell trajectory on torus structures samples the complete speed versus direction phase space (Figure S7, Supporting Information), again demonstrating that cells dynamically adjust their migration mode depending on k .

3. Conclusion

Prior works indicated that cells are able to sense isotropic substrate curvatures (e.g., on spherical structures) and make functional decisions (e.g., differentiation, migration) accordingly. The current study discovers that, on anisotropic curved structures, such ability to sense substrate curvature leads to unexpected migration behaviors in terms of directionality, persistence, and speed. Moreover, the migration mode in each instance is dynamically governed by the substrate curvature that is perceived by the cell. This fundamental insight not only corroborates previously described cell behaviors on isotropic curved geometries, but also explains cell behaviors on complex anisotropic structures and can help us better predict cell response in physiologically relevant 3D *in vitro* and *in vivo* environments. Furthermore, this might offer new strategies for the informed structural design of cell-instructive features that control cell recruitment into porous implantable biomaterials.

On convex cylindrical substrates, the curvature that the cells perceive constantly varies along the migration trajectories and depends on the principal curvature of the cylinder and the migration direction. Both migration speed and persistence are dynamically adapted in response to this direction-dependent perceived curvature. Minimization of bending of the cell body on convex cylindrical substrates leads to cell alignment in the uncurved, longitudinal direction. Deviation from this direction forces the cell to adapt to a more bent configuration, which is accompanied by a lower migration speed and which drives the cell to turn back toward the uncurved longitudinal direction. Overall, the continuous dynamic adjustment of cell migration toward direction of least curvature results in a persistent and directed migration behavior along the convex cylinder axis. On the other hand, on concave cylindrical surfaces, an additional parameter plays a role in how cells perceive the substrate curvature. Cells lift their cell body upward, off the substrate, to effectively minimize bending of the cell body that is otherwise enforced by the curvature of the substrate. Since cells can avoid the substrate curvature irrespective of their orientation on the cylinder, a directive orientation cue is absent on concave cylindrical substrates. This coping mechanism results in a migration mode characterized by fast but undirected and low-persistence migration. These distinct migration modes therefore reveal a separation between migration speed and persistence that appears only in the presence of mesoscale substrate curvature (i.e., not in previously studied migration on 2D substrates). On geometrical structures that contain both convex and concave curvatures in orthogonal directions, migration speed was direction-dependent and cells orient in the direction where they can most effectively avoid bending. Thus, curvature-guided migration is not initiated by a preference for a certain substrate curvature (i.e., preference driven), instead it is avoidance-driven as cells migrate in the direction where they can most effectively avoid the substrate curvature. Together, these findings highlight that cellular orientation and attachment morphology strongly affect the cell-perceived substrate curvature on anisotropic curved geometries, which in turn determines the cell's migration behavior.

4. Experimental Section

Design and Production of Cell Culture Chips: Cell culture chips containing 3D curved structures were created with PDMS using a molding process. Chip molds were designed using computer-aided design software (Rhino 3D, McNeel Europe, Barcelona, Spain). The molds were produced in glass slides by FEMTOPrint (Muzzano, Switzerland). The chips contain convex and concave cylindrical structures with diameters $d = 250, 350, 500, 750,$ and $1000 \mu\text{m}$ (corresponding to principal curvatures in the circumferential direction $\kappa = 2/d = 1/125, 1/175, 1/250, 1/375, 1/500 \mu\text{m}^{-1}$) and a length of 1 mm, as well as the saddle point area of torus structures with a circumferential diameter of $750 \mu\text{m}$. Concave surfaces are defined with a negative curvature; convex surfaces with a positive curvature. The chip mold was exposed to tridecafluoro(1,1,2,2-tetrahydrooctyl)trichlorosilane vapor (abcr GmbH, Karlsruhe, Germany) to facilitate smooth removal of PDMS from the mold. PDMS (Sylgard 184, 1:10 crosslinker:monomer ratio, Dow Corning, Midland, USA) was cast on the mold and cured overnight at 65°C . The stiffness of the PDMS substrate was expected to be around $1.5\text{--}2 \text{ MPa}$.^[46] At this stiffness, the PDMS substrate could be regarded as “undeformable” by cell forces. To ensure a smooth surface, a thin additional PDMS layer was superimposed after curing, as previously described.^[23] The surface roughness of the chip was characterized in the previous work.^[47] Cell culture chips were exposed to O_2 plasma and coated with $50 \mu\text{g mL}^{-1}$ bovine fibronectin (tebu-bio, Heerhugowaard, Netherlands) for 1.5 h prior to cell seeding.

hBMSC Culture: hBMSCs were cultured in expansion medium consisting of Dulbecco's modified Eagle's medium (Sigma-Aldrich, St. Louis, USA) supplemented with 10% fetal bovine serum (Biochrom GmbH, Berlin, Germany), 1% penicillin/streptomycin (Biochrom GmbH, Berlin, Germany), and 1% L-glutamine (glutaMAX, Invitrogen, Carlsbad, USA). When a confluency of 80% was reached, cells were trypsinized, stained in suspension with $10 \mu\text{M}$ CellTracker Green (Life Technologies, Carlsbad, USA), and seeded (3×10^4 cells mL^{-1}) on the fibronectin-coated chip. In this study, single-cell migration was focused on and low-cell-density cultures were used to limit cell–cell contact. The cell density was constant across all tested structures. Cells were cultured on the chips for 3 h at 37°C and 5% CO_2 to allow for cell adhesion before the start of the time-lapse imaging.

Time-Lapse Imaging of Migrating Cells: The chip with the attached cells was transferred to a microscopy dish and placed on a Leica TCS SP5 microscope equipped with an incubator chamber that allowed for long-term imaging at 37°C and 5% CO_2 . Cells were imaged with a $20\times, 0.7 \text{ NA}$ objective, and a white-light laser (Supercontinuum Fiber Laser, Leica, Wetzlar, Germany) at an excitation wavelength of 488 nm. Multiple cylindrical and toroidal structures (3 structures per experimental group, in total 15 convex cylinders, 15 concave cylinders, and 3 toroidal structures) and 3 flat areas on the chip were imaged using a motorized stage. Z-stacks of the top areas of the cylinders ($\approx 40\%$ of the radius of the cylinder) were recorded with $3 \mu\text{m}$ z-spacing every 45 min for 48 h. This was done to ensure that the analysis of cell trajectories could be performed using the projected images (on the $x\text{--}y$ plane) with negligible displacement in the z -direction. This approximation significantly accelerated the trajectory analysis and only resulted in an error in the determination of migration orientation of less than 0.1%; thus, the z -displacement could be safely neglected without any mathematical correction.

Cell Migration Analysis: The centroid of the cells were tracked manually using ImageJ plugin MtrackJ,^[48] yielding the 3D trajectories $\mathbf{r}_i(t) \equiv \{x_i(t), y_i(t), z_i(t)\}$ of cells as a function of time t for each detected cell $i = 1, 2, \dots, n$, where $n \geq 26$ in each experimental group (i.e., each substrate structure). As a measure of the migration anisotropy, the ratio dx/dy was introduced as an anisotropy index, where dx and dy are defined as the largest distance covered by the cell in the x - and y -directions, respectively. The x -axis was defined as the longitudinal axis of the cylinders, whereas the y -axis was defined as the horizontal direction perpendicular to the cylinder axis. Migration speed was calculated $v(t) = |d\mathbf{r}(t)|/dt$, where $d\mathbf{r}(t) = \mathbf{r}(t+1) - \mathbf{r}(t)$ and dt denotes the timeframe

interval. The time-dependent migration orientation θ was calculated as $\theta(t) = \cos^{-1}(\mathbf{d}\bar{r}(t)/|\mathbf{d}\bar{r}(t)|)$, where $\mathbf{d}\bar{r}(t)$ denotes the projected displacement vector on the x - y plane. A track segment is considered to be “aligned” when $|\theta| < 30^\circ$ and “non-aligned” otherwise. Turn angle was calculated as $d\theta(t) = \theta(t+1) - \theta(t)$. A track segment is considered to be “persistent” when $|d\theta(t) - d\theta(t-1)| < 30^\circ$. Persistence time t_p is defined as the duration over which persistent migration is maintained. To statistically assess the trajectory evolution, probabilistic kymographs of the cell states were constructed using segmental trajectory analysis as described previously for analysis of peptide conformational dynamics.^[49] Briefly, from the ensemble trajectories, segments were selected on the basis of migration features of interest (e.g., migration direction) and were considered as independent starting points in the analysis, thus effectively segmenting the trajectories into shorter experiments, all starting with a state of interest. The dynamics subsequent to this particular state was then analyzed by averaging the parameter of interest as a function of elapsed time Δt . All trajectory analyses were performed using a custom-written script in MATLAB (The Mathworks Inc.).

Live Imaging of the F-Actin Cytoskeleton: Cells were seeded on the fibronectin-coated cell culture chip, and 100 nM SiR-actin dye (Spirochrome, Stein am Rhein, Switzerland) was added to the medium. Cells were incubated with the dye overnight. The cell culture chip was transferred to a microscopy dish filled with fresh culture medium + 100 nM SiR-actin dye. Actin dynamics in hBMSCs migrating on concave cylindrical surfaces, convex cylindrical surfaces, and flat surfaces were imaged at 37 °C and 5% CO₂ using a Leica TCS SP5 microscope with a 20 ×, 0.7 NA objective with 1.5 digital zoom and a white light laser set at an excitation wavelength of 652 nm. Z-stacks with 3 μm z-spacing were recorded every 20 min for 24 h.

Immunohistochemistry: hBMSCs were seeded on a fibronectin-coated chip and cultured for 24 h. Cells were then fixed in 3.7% formaldehyde and stained for F-actin with phalloidin (Phalloidin-Atto 488, Sigma-Aldrich, St. Louis, USA). Structures were imaged using a Leica TCS SP5 microscope with a 20 ×, 0.7 NA objective. Z-stacks of the top areas of the cylinders (≈40% of the radius of the cylinder) with 3 μm z-spacing were recorded. F-actin fiber orientation was quantified from the maximum projection images using the OrientationJ plug-in (Biomedical Imaging Group, Ecole Polytechnique Federale de Lausanne, Switzerland, <http://bigwww.epfl.ch/demo/orientation/>) in ImageJ. For each experimental group, three images were analyzed.

Statistical Analysis: Unless otherwise stated in the figure legend, the data presented here are expressed as mean ± 95% confidence interval. The numbers of samples analyzed are indicated in the figure legends. Non-parametric Kruskal–Wallis test with Dunn’s multiple comparison post hoc test was performed using Prism (GraphPad) or MATLAB to assess differences in the migration parameters between the concave and convex surfaces, the cylindrical surfaces of different sizes, and the migration directions. The ranges of p -values are indicated in the figure legends.

Supporting Information

Supporting Information is available from the Wiley Online Library or from the author.

Acknowledgements

The authors acknowledge the support from the Netherlands Cardio Vascular Research Initiative: The Dutch Heart Foundation, Dutch Federation of University Medical Centers, the Netherlands Organization for Health Research and Development, and the Royal Netherlands Academy of Sciences; and the support by the Dutch Ministry of Education, Culture and Science for the Gravitation Program 024.003.103 “Materials Driven Regeneration.” The authors further acknowledge funding from the Berlin-Brandenburg Center for Regenerative Therapies

(BCRT) for A.P. The authors would like to thank the BCRT Core Unit “Cell Harvesting” for providing the mesenchymal stromal cells (hBMSCs) used in this study.

Conflict of Interest

The authors declare no conflict of interest.

Keywords

cell adhesion, cell migration, persistence, substrate curvature, tissue geometry

Received: March 22, 2019

Revised: August 16, 2019

Published online: September 5, 2019

- [1] A. T. Nguyen, S. R. Sathe, E. K. F. Yim, *J. Phys.: Condens. Matter* **2016**, *28*, 183001.
- [2] V. Ruprecht, P. Monzo, A. Ravasio, Z. Yue, E. Makhija, P. O. Strale, N. Gauthier, G. V. Shivashankar, V. Studer, C. Albiges-rizo, V. Viasnoff, *J. Cell Sci.* **2017**, *130*, 51.
- [3] M. Nikkhah, F. Edalat, S. Manoucheri, A. Khademhosseini, *Biomaterials* **2012**, *33*, 5230.
- [4] N. A. Kurniawan, P. K. Chaudhuri, C. T. Lim, *J. Biomech.* **2016**, *49*, 1355.
- [5] A. I. Teixeira, G. A. Abrams, P. J. Bertics, C. J. Murphy, P. F. Nealey, *J. Cell Sci.* **2003**, *116*, 1881.
- [6] A. Ray, O. Lee, Z. Win, R. M. Edwards, P. W. Alford, D. Kim, P. P. Provenzano, *Nat. Commun.* **2017**, *8*, 14923.
- [7] B. Zimerman, M. Arnold, J. Ulmer, J. Bl, A. Besser, J. P. Spatz, B. Geiger, *IEE Proc. Nanobiotech.* **2004**, *151*, 62.
- [8] G. R. R. Juan, P. W. Oakes, M. L. Gardel, *Mol. Biol. Cell* **2017**, *28*, 1043.
- [9] H. G. Yevick, G. Duclos, I. Bonnet, P. Silberzan, *Proc. Natl. Acad. Sci. U. S. A.* **2015**, *112*, 5944.
- [10] G. A. Dunn, J. P. Heath, *Exp. Cell Res.* **1976**, *101*, 1.
- [11] K.-H. Nam, P. Kim, D. K. Wood, S. Kwon, P. P. Provenzano, D.-H. Kim, *Sci. Rep.* **2016**, *6*, 29749.
- [12] P. P. Provenzano, K. W. Eliceiri, J. M. Campbell, D. R. Inman, J. G. White, P. J. Keely, *BMC Med.* **2006**, *4*, 38.
- [13] P. P. Provenzano, D. R. Inman, K. W. Eliceiri, J. G. Knittel, L. Yan, C. T. Rueden, J. G. White, P. J. Keely, *BMC Med.* **2008**, *6*, 11.
- [14] L. A. Bentolila, R. Prakash, D. Mihic-probst, M. Wadehra, H. K. Kleinman, T. S. Carmichael, B. Péault, R. L. Barnhill, C. Lugassy, *Sci. Rep.* **2016**, *6*, 23834.
- [15] P. G. Gritsenko, O. Ilina, P. Friedl, *J. Pathol.* **2012**, *226*, 185.
- [16] B. Weigelin, G. Bakker, P. Friedl, *IntraVital* **2012**, *1*, 32.
- [17] I. K. Ko, S. J. Lee, A. Atala, J. J. Yoo, *Exp. Mol. Med.* **2013**, *45*, e57.
- [18] J. Y. Park, D. H. Lee, E. J. Lee, S.-H. Lee, *Lab Chip* **2009**, *9*, 2043.
- [19] M. Werner, S. B. G. Blanquer, S. P. Haimi, G. Korus, J. W. C. Dunlop, G. N. Duda, D. W. Grijpma, A. Petersen, *Adv. Sci.* **2017**, *4*, 1600347.
- [20] N. D. Bade, T. Xu, R. D. Kamien, R. K. Assoian, K. J. Stebe, *Biophys. J.* **2018**, *114*, 1467.
- [21] L. Pieuchot, J. Marteau, A. Guignandon, T. Dos Santos, I. Brigaud, P. Chauvy, T. Cloatre, A. Ponche, T. Petithory, P. Rougerie, M. Vassaux, J. Milan, N. T. Wakhloo, A. Spangenberg, M. Bigerelle, K. Anselme, *Nat. Commun.* **2018**, *9*, 3995.
- [22] N. D. Bade, R. D. Kamien, R. K. Assoian, K. J. Stebe, *Sci. Adv.* **2017**, *3*, e1700150.

- [23] M. Werner, N. A. Kurniawan, G. Korus, C. V. C. Bouten, A. Petersen, *J. R. Soc., Interface* **2018**, *15*, 20180162.
- [24] E. L. S. Fong, C. K. Chan, S. B. Goodman, *Biomaterials* **2011**, *32*, 395.
- [25] P. Maiuri, J.-F. Rupprecht, S. Wieser, V. Ruprecht, O. Bénichou, N. Carpi, M. Coppey, S. de Beco, N. Gov, C.-P. Heisenberg, C. Lage Crespo, F. Lautenschlaeger, M. le Berre, A.-M. Lennon-Dumenil, M. Raab, H.-R. Thiam, M. Piel, M. Sixt, R. Voituriez, *Cell* **2015**, *161*, 374.
- [26] Y. Y. Biton, S. A. Safran, *Phys. Bio.* **2009**, *6*, 046010.
- [27] J. A. Sanz-Herrera, P. Moreo, J. M. García-Aznar, M. Doblaré, *Biomaterials* **2009**, *30*, 6674.
- [28] D. A. Lauffenburger, A. F. Horwitz, *Cell* **1996**, *84*, 359.
- [29] B. Sun, R. H. W. Lam, *2016 IEEE 16th Int. Conf. Nanotechnol.* **2016**, *1*, 339.
- [30] T. Yamashita, P. Kollmannsberger, K. Mawatari, T. Kitamori, V. Vogel, *Acta Biomater.* **2016**, *45*, 85.
- [31] C. de Pascalis, S. Etienne-Manneville, *Mol. Biol. Cell* **2017**, *28*, 1833.
- [32] X. He, Y. Jiang, *Phys. Bio.* **2017**, *14*, 035006.
- [33] R. A. Denu, S. Nemcek, D. D. Bloom, D. A. Goodrich, J. Kim, D. F. Mosher, P. Hematti, *Acta Haematol.* **2016**, *136*, 85.
- [34] E. S. Fioretta, M. Simonet, A. I. P. M. Smits, F. P. T. Baaijens, C. V. C. Bouten, *Biomacromolecules* **2014**, *15*, 821.
- [35] D. Jones, D. Park, M. Anghelina, T. Pécot, R. Machiraju, R. Xue, J. J. Lannutti, J. Thomas, S. L. Cole, L. Moldovan, N. I. Moldovan, *Biomaterials* **2015**, *52*, 395.
- [36] L. Dupré, R. Houmadi, C. Tang, J. Rey-Barroso, *Front. Immunol.* **2015**, *6*, 586.
- [37] K. H. Song, S. J. Park, D. S. Kim, J. Doh, *Biomaterials* **2015**, *51*, 151.
- [38] W. Xi, S. Sonam, T. B. Saw, B. Ladoux, C. T. Lim, *Nat. Commun.* **2017**, *8*, 1517.
- [39] F. A. Maechler, C. Allier, A. Roux, C. Tomba, *J. Cell Sci.* **2019**, *132*, jcs222372.
- [40] S. H. Kim, G. Lee, S. Park, *Int. J. Mech. Sys. Eng.* **2015**, *1*, 104.
- [41] T. Gong, K. Zhao, G. Yang, J. Li, H. Chen, Y. Chen, *Adv. Healthcare Mater.* **2014**, *3*, 1608.
- [42] S. Watari, K. Hayashi, J. A. Wood, P. Russell, P. F. Nealey, C. J. Murphy, D. C. Genetos, *Biomaterials* **2012**, *33*, 128.
- [43] S. B. G. Blanquer, M. Werner, M. Hannula, S. Sharifi, G. P. R. Lajoinie, D. Eglin, J. Hyttinen, A. A. Poot, D. W. Grijpma, *Biofabrication* **2017**, *9*, 025001.
- [44] S. Rajagopalan, R. A. Robb, *Med. Image Anal.* **2006**, *10*, 693.
- [45] F. P. W. Melchels, K. Bertoldi, R. Gabbriellini, A. H. Velders, J. Feijen, D. W. Grijpma, *Biomaterials* **2010**, *31*, 6909.
- [46] I. D. Johnston, D. K. McCluskey, C. K. L. Tan, M. C. Tracey, *J. Micro-mech. Microeng.* **2014**, *24*, 035017.
- [47] M. Werner, N. A. Kurniawan, G. Korus, C. V. C. Bouten, A. Petersen, *R. Soc. Collect.* **2018**, <https://doi.org/10.6084/m9.figshare.c.4174829>.
- [48] E. Meijering, O. Dzyubachyk, I. Smal, *Methods Enzymol.* **2012**, *504*, 183.
- [49] S. Enemark, N. A. Kurniawan, R. Rajagopalan, *Sci. Rep.* **2012**, *2*, 649.